Hindawi Publishing Corporation
Advances in Mechanical Engineering
Volume 2014, Article ID 359872, 16 pages
http://dx.doi.org/10.1155/2014/359872

Research Article

First and Second-Law Efficiency Analysis and ANN Prediction of a Diesel Cycle with Internal Irreversibility, Variable Specific Heats, Heat Loss, and Friction Considerations

M. M. Rashidi,[1,2] A. Hajipour,[3] A. Mousapour,[4] M. Ali,[5] Gongnan Xie,[6] and N. Freidoonimehr[7]

[1] *Mechanical Engineering Department, Engineering Faculty of Bu-Ali Sina University, Hamedan 651754161, Iran*
[2] *Mechanical Engineering Department, University of Michigan-Shanghai Jiao Tong University Joint Institute, Shanghai Jiao Tong University, Shanghai 201101, China*
[3] *Young Researchers and Elite Club, Ayatollah Amoli Branch, Islamic Azad University, Amol 4615143358, Iran*
[4] *Department of Mechanical Engineering, Science and Research Branch, Islamic Azad University, Tehran 1477893855, Iran*
[5] *Mechanical Engineering Department, College of Engineering, King Saud University, P.O. Box 800, Riyadh 11421, Saudi Arabia*
[6] *School of Mechanical Engineering, Northwestern Polytechnical University, Xi'an, Shaanxi 710072, China*
[7] *Young Researchers and Elite Club, Hamedan Branch, Islamic Azad University, Hamedan 6518115743, Iran*

Correspondence should be addressed to M. Ali; mali@ksu.edu.sa

Received 27 January 2014; Revised 13 March 2014; Accepted 18 March 2014; Published 24 April 2014

Academic Editor: Jiin Y. Jang

The variability of specific heats, internal irreversibility, heat and frictional losses are neglected in air-standard analysis for different internal combustion engine cycles. In this paper, the performance of an air-standard Diesel cycle with considerations of internal irreversibility described by using the compression and expansion efficiencies, variable specific heats, and losses due to heat transfer and friction is investigated by using finite-time thermodynamics. Artificial neural network (ANN) is proposed for predicting the thermal efficiency and power output values versus the minimum and the maximum temperatures of the cycle and also the compression ratio. Results show that the first-law efficiency and the output power reach their maximum at a critical compression ratio for specific fixed parameters. The first-law efficiency increases as the heat leakage decreases; however the heat leakage has no direct effect on the output power. The results also show that irreversibilities have depressing effects on the performance of the cycle. Finally, a comparison between the results of the thermodynamic analysis and the ANN prediction shows a maximum difference of 0.181% and 0.194% in estimating the thermal efficiency and the output power. The obtained results in this paper can be useful for evaluating and improving the performance of practical Diesel engines.

1. Introduction

The cycle experienced in the cylinder of an internal combustion engine is very complex; to make the analysis of an engine cycle much more manageable, the real cycle is approximated with an ideal air-standard cycle, which differs from the actual one by some aspects. Variable specific heat of the working fluid, internal irreversibility, heat transfer through the cylinder wall, and friction are factors that affect the engine performance, whereas they are neglected in dealing with thermodynamic analysis of ideal air-standard cycles. The Diesel cycle is the ideal air-standard cycle for CI reciprocating engines. The CI engine, first proposed by Rudolph Diesel in the 1890s, is very similar to the SI engine, differing mainly in the method of initiating combustion [1–3]. In recent years, several attentions have been paid to the performance of internal combustion engines for different cycles. Effects of friction and temperature-dependent specific heat of the working fluid on the performance of a Diesel engine have been performed by Al-Sarkhi et al. [4]. Performance analysis of air-standard Diesel cycle using an alternative irreversible heat transfer approach has been investigated by Al-Hinti et

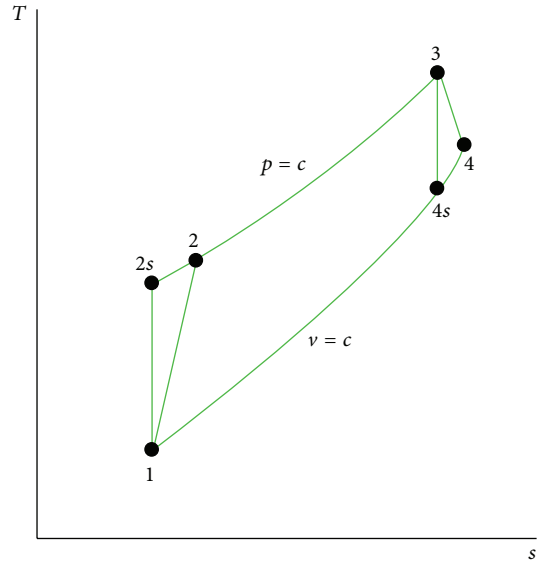

Figure 1: The T-s diagram for an air-standard Diesel cycle.

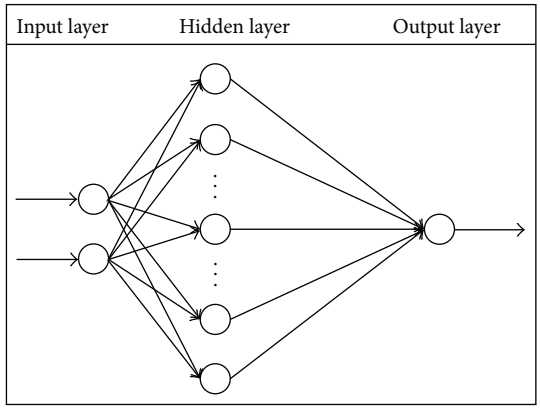

Figure 2: A diagram of a MLFF neural network.

al. [5]. Reciprocating heat-engine cycles have been done by Ge et al. [6]. Power, efficiency, entropy-generation rate, and ecological optimization for a class of generalized irreversible universal heat-engine cycles have been studied by Chen et al. [7]. Heat loss as a percentage of fuels energy in air-standard Otto and Diesel cycles has been performed by Ozsoysal [8]. Comparative performance analysis of irreversible Dual and Diesel cycles under maximum power conditions has been investigated by Parlak [9]. Second-law analyses applied to internal combustion engines operation have been presented by Rakopoulos and Giakoumis [10]. Energy, exergy, and second-law performance criteria have been studied by Lior and Zhang [11]. Thermodynamic irreversibilities and exergy balance in combustion processes have been reported by Som and Datta [12]. Second-law analysis of an ideal Otto cycle has been performed by Lior and Rudy [13]. First- and second-law analysis of an ejector expansion Joule-Thomson cryogenic refrigeration cycle and first- and second-laws analysis of an air-standard Dual cycle with heat loss consideration have been investigated by Rashidi et al. [14, 15]. Finite-time thermodynamic modelling and analysis of an irreversible Otto and Dual cycles have been studied by Ge et al. [16, 17]. Performance analysis of a Diesel cycle under the restriction of maximum cycle temperature with considerations of heat loss, friction, and variable specific heats has been done by Hou and Lin [18] and correct evaluation of effects of heat transfer on the exergy efficiency of an air-standard Otto cycle has been performed by Rashidi et al. [19]. During recent decades, some different studies have been performed about the applications of AI (artificial intelligence) methods, especially ANN (artificial neural network), in thermodynamics. Kalogirou [20] applied AL techniques to model and predict the performance and the control of combustion process. Furthermore, Deh Kiani et al. [21] have presented a paper about ANN modeling of a spark ignition engine for predicting the engine brake power, output torque, and exhaust emissions of the engine. In addition, Gandhidasan and Mohandes [22] have proposed the application of ANN-based model for simulation of the relationship between the inlet and outlet parameters of a dehumidifier. They applied a multilayer ANN for dehumidifier performance investigation. Moreover, some ANN models have been presented in order to predict the fresh steam properties from a brown coal-fired boiler of a power plant by Smrekar et al. [23] using real plant data. Rashidi et al. [24] illustrated the parametric analysis and optimization of entropy generation in unsteady MHD flow past a stretching rotating disk using artificial neural network (ANN) and particle swarm optimization (PSO) algorithm. In another study, Rashidi et al. [25] performed the parametric study and optimization of regenerative Clausius and organic Rankine cycles with two feedwater heaters. They proposed a procedure based on the combination of ANN and artificial bees colony (ABC). They have selected thermal efficiency, exergy efficiency, and specific work as the objective functions of optimization and have evaluated the mentioned parameters for different values of the outlet pressures from the second and third pumps and finally Rashidi et al. [26], using artificial neural networks and genetic algorithms, analyzed and optimized a transcritical power cycle with regenerator.

In this study, the effects of various parameters of irreversibility such as internal irreversibility (compression and expansion efficiencies), variable specific heats of the working fluid, heat loss, and friction on the first-law and the second-law efficiency of Diesel cycle are investigated. In addition to that, ANN is employed to predict the thermal efficiency and power output values of the considered Diesel cycle versus the minimum and maximum temperatures as well as the compression ratio.

2. Thermodynamic Analysis

2.1. First-Law Efficiency Analysis. Since thermodynamic analysis of internal combustion engines in practical conditions is extremely complex, for this reason the real cycles are approximated with ideal air-standard cycles by applying a number of assumptions. The T-s diagram for an air-standard Diesel cycle is shown in Figure 1. It can be seen that the compression processes ($1 \rightarrow 2s$) and ($1 \rightarrow 2$) are

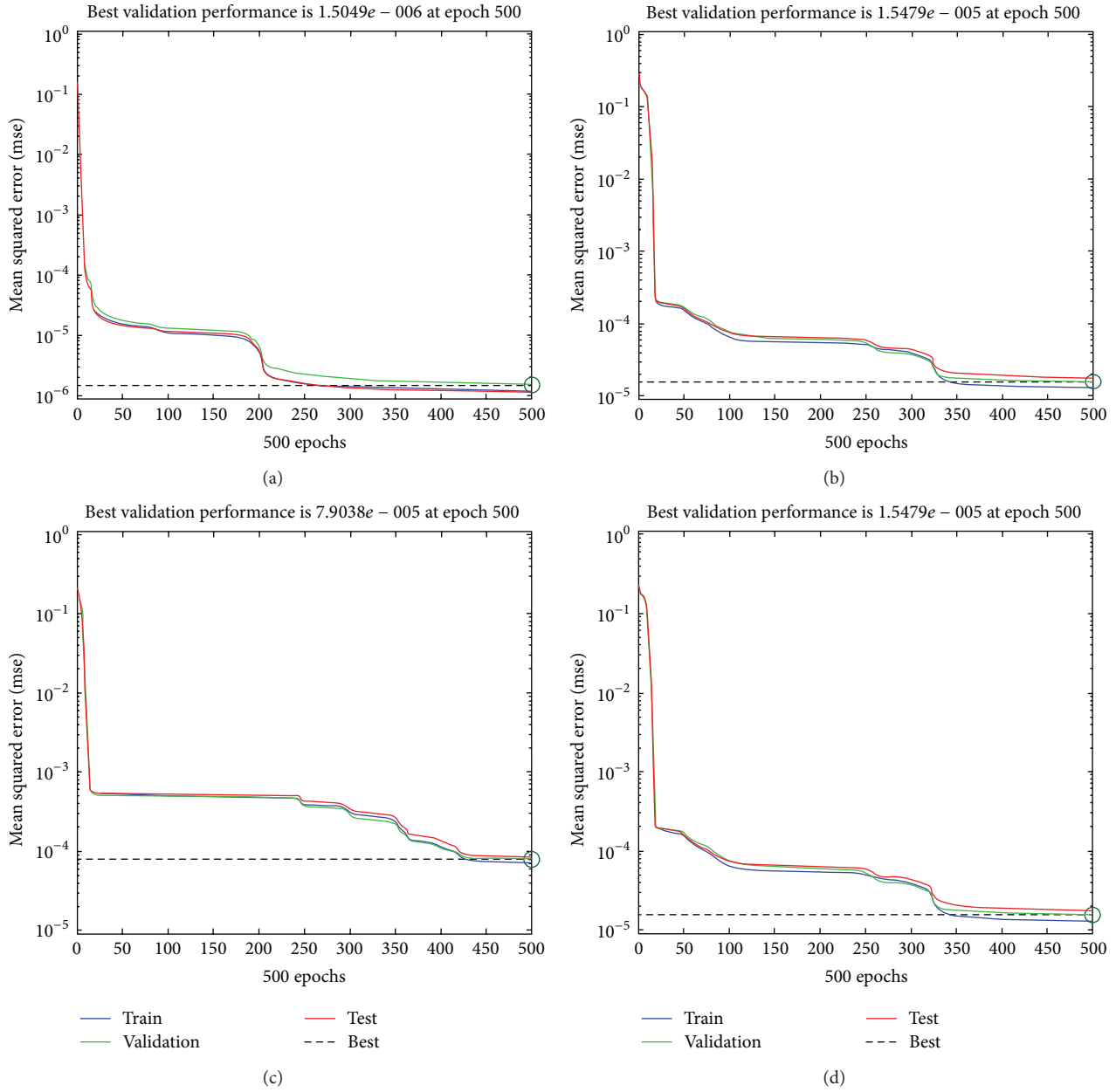

Figure 3: Training procedures of interpolation part using BEP with respect to (a) minimum temperature and compression ratio for power output; (b) minimum temperature and compression ratio for thermal efficiency; (c) maximum temperature and compression ratio for power output; (d) maximum temperature and compression ratio for thermal efficiency.

reversible and irreversible adiabatic processes, respectively. The heat addition process ($2 \rightarrow 3$) is an isobaric process; the expansion processes ($3 \rightarrow 4s$) and ($3 \rightarrow 4$) are reversible and irreversible adiabatic processes, respectively. The cycle is completed by an isochoric heat rejection process ($4 \rightarrow 1$). In the air-standard analysis, the working fluid is assumed to behave as an ideal gas with constant specific heats. But, this assumption can be valid only for the small temperature ranges during the cycle. For the large temperature range of $300 \rightarrow 2000$ K, this assumption cannot be applied, because it causes considerable errors. Hence, with a suitable approximation, the specific heats of the working fluid can be written as linear functions of temperature [16]:

$$C_p = a_p + k_1 T,$$
$$C_v = b_v + k_1 T, \tag{1}$$

where a_p, b_v, and k_1 are constants and C_p and C_v are the specific heats at constant pressure and constant volume, respectively. Due to the relation between the specific heats, one can obtain the working fluid gas constant as [4]

$$R = C_p - C_v = a_p - b_v. \tag{2}$$

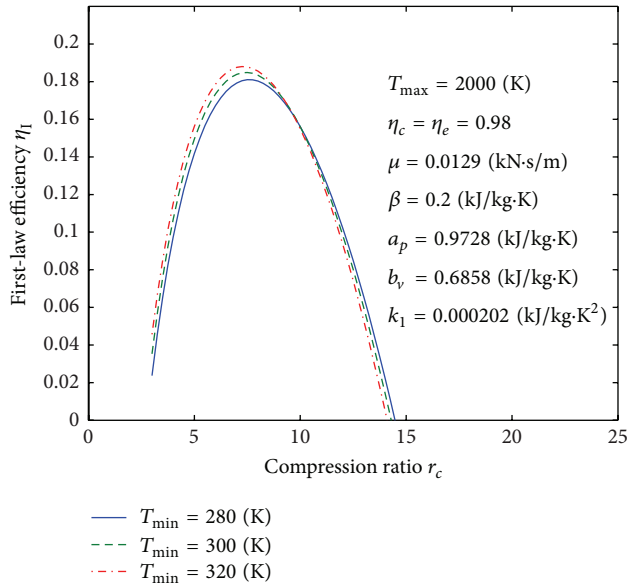

FIGURE 4: Influence of T_{min} on curves of the first-law efficiency versus the compression ratio.

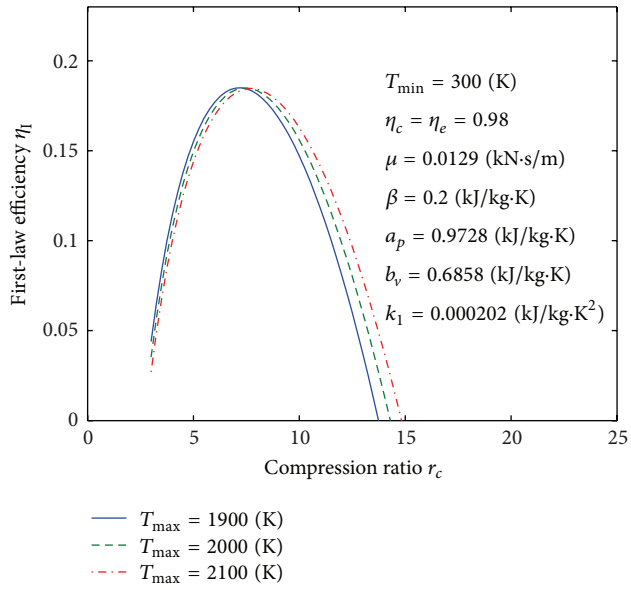

FIGURE 5: Influence of T_{max} on curves of the first-law efficiency versus the compression ratio.

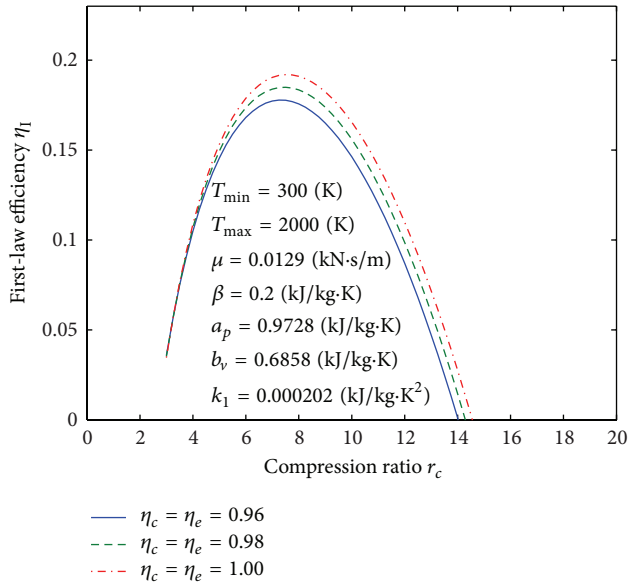

FIGURE 6: Influence of η_c and η_e on curves of the first-law efficiency versus the compression ratio.

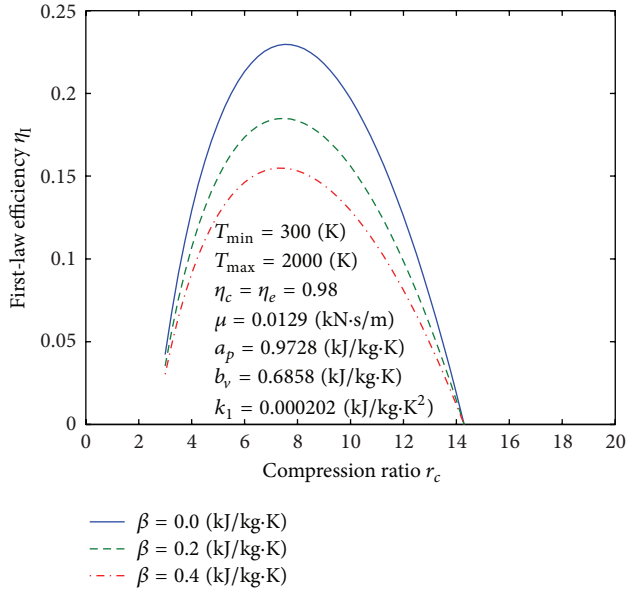

FIGURE 7: Influence of β on curves of the first-law efficiency versus the compression ratio.

As it can be seen in Figure 1, in the ideal air-standard Diesel cycle, for the reversible adiabatic compression ($1 \rightarrow 2s$) and expansion ($3 \rightarrow 4s$) processes, the entropy generation and thus the entropy change of the working fluid are zero, while as in a real Diesel cycle, the irreversibilities cause the entropy of the working fluid to increase, during the irreversible adiabatic compression ($1 \rightarrow 2$) and expansion ($3 \rightarrow 4$) processes. Therefore, the following compression and expansion efficiencies can be used to describe the internal irreversibilities of the compression and expansion processes, respectively, [19]

$$\eta_c = \frac{\int_1^{2s} C_v dT}{\int_1^{2} C_v dT} = \frac{\int_1^{2s} (b_v + k_1 T)\, dT}{\int_1^{2} (b_v + k_1 T)\, dT} \approx \frac{T_{2s} - T_1}{T_2 - T_1}, \quad (3)$$

$$\eta_e = \frac{\int_3^{4} C_v dT}{\int_3^{4s} C_v dT} = \frac{\int_3^{4} (b_v + k_1 T)\, dT}{\int_3^{4s} (b_v + k_1 T)\, dT} \approx \frac{T_4 - T_3}{T_{4s} - T_3}. \quad (4)$$

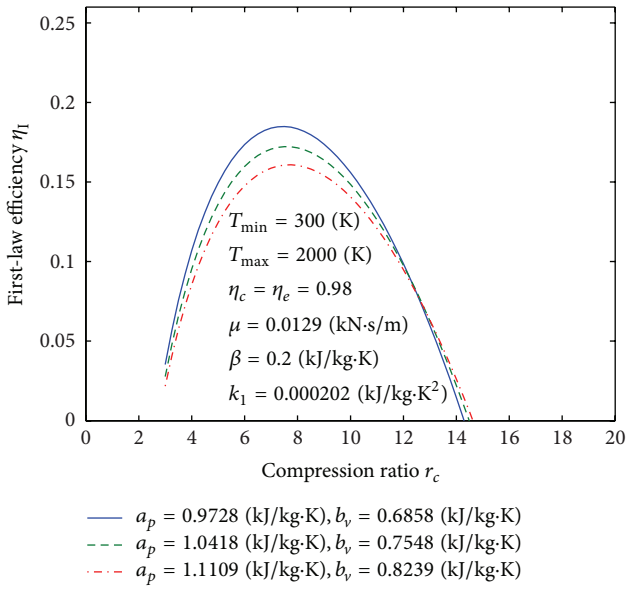

FIGURE 8: Influence of a_p and b_v on curves of the first-law efficiency versus the compression ratio.

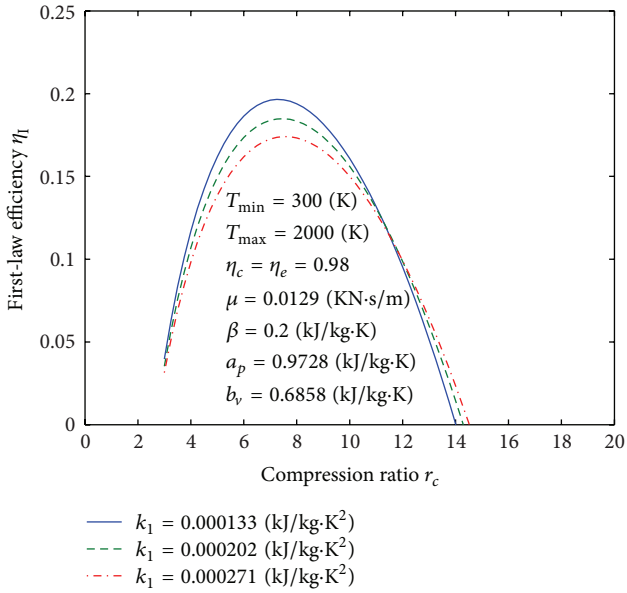

FIGURE 9: Influence of k_1 on curves of the first-law efficiency versus the compression ratio.

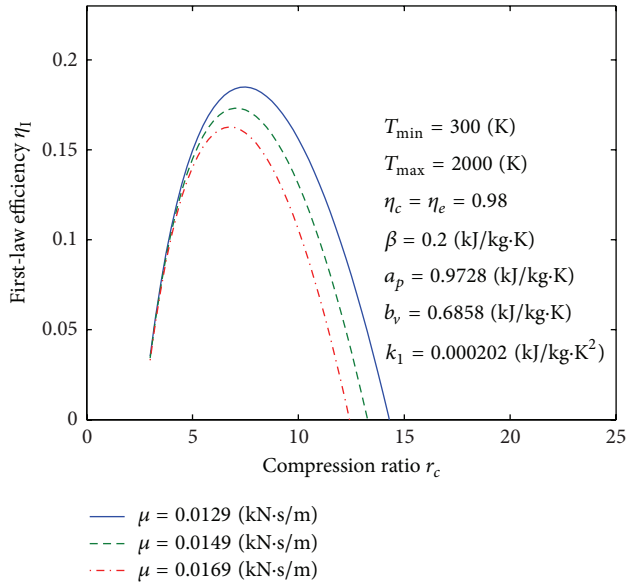

FIGURE 10: Influence of μ on curves of the first-law efficiency versus the compression ratio.

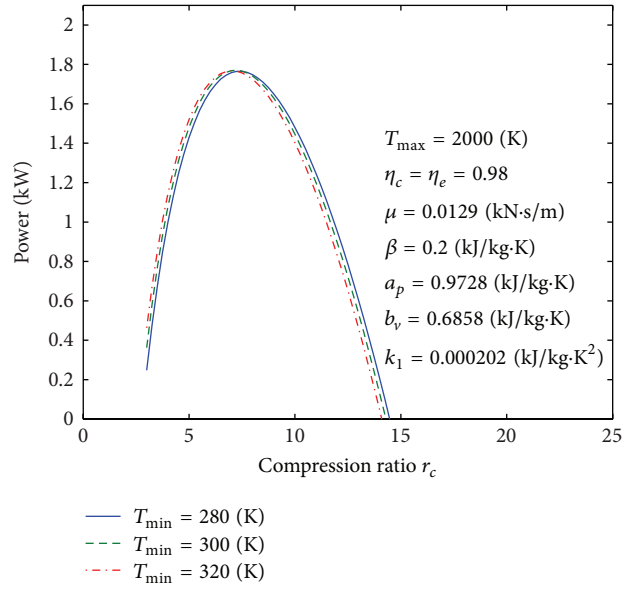

FIGURE 11: Influence of T_{min} on curves of the power output versus the compression ratio.

The heat added per second in the isobaric heat addition process (2 → 3) may be written as

$$\begin{aligned} Q_{in} &= NM\left(\int_{T_2}^{T_3} C_p dT\right) \\ &= NM\int_{T_2}^{T_3}\left(a_p + k_1 T\right)dT \\ &= NM\left[a_p\left(T_3 - T_2\right) + 0.5k_1\left({T_3}^2 - {T_2}^2\right)\right]. \end{aligned} \tag{5}$$

The heat rejected per second in the isochoric heat-rejection process (4 → 1) may be written as

$$\begin{aligned} Q_{out} &= NM\left(\int_{T_1}^{T_4} C_v dT\right) \\ &= NM\int_{T_1}^{T_4}\left(b_v + k_1 T\right)dT \\ &= NM\left[b_v\left(T_4 - T_1\right) + 0.5k_1\left({T_4}^2 - {T_1}^2\right)\right], \end{aligned} \tag{6}$$

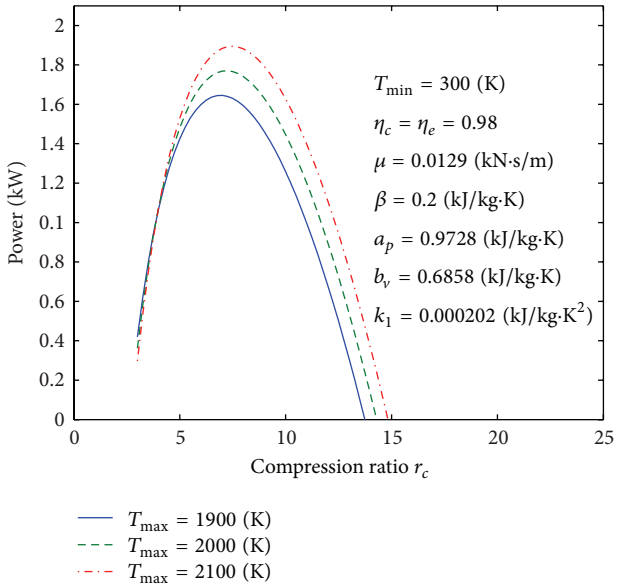

FIGURE 12: Influence of T_{max} on curves of the power output versus the compression ratio.

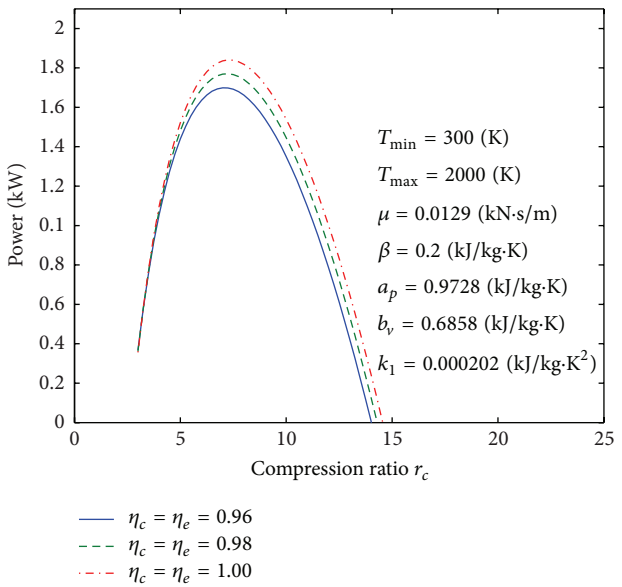

FIGURE 13: Influence of η_c and η_e on curves of the power output versus the compression ratio.

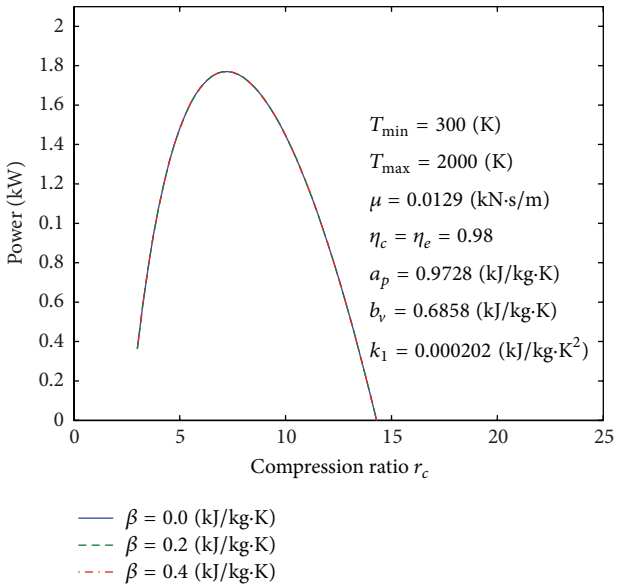

FIGURE 14: Influence of β on curves of the power output versus the compression ratio.

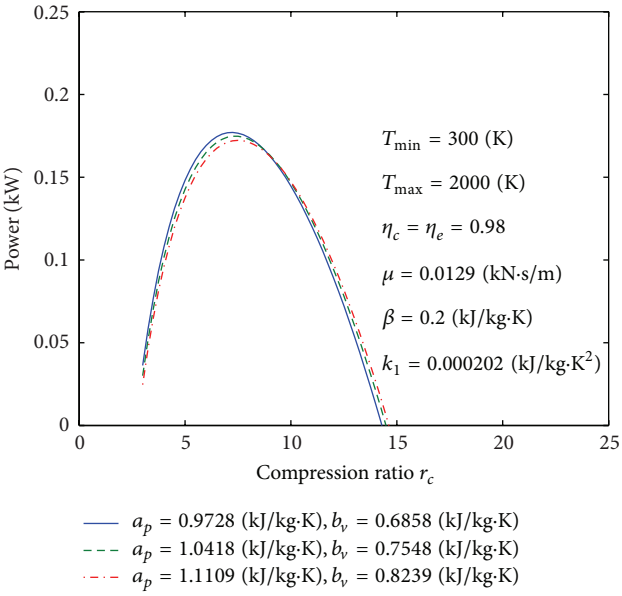

FIGURE 15: Influence of a_p and b_v on curves of the power output versus the compression ratio.

where M is the mass of the working fluid and N is cycles per second.

The entropy changes for a reversible process ($i \rightarrow j$) as follows:

$$\int_i^j ds = \int_i^j C_v \frac{dT}{T} + \int_i^j R \frac{dV}{V}. \tag{7}$$

Plug (3) for C_v into (7), for the compression and expansion isentropic processes, we have

$$\begin{aligned} k_1 (T_{2s} - T_1) + b_v \ln\left(\frac{T_{2s}}{T_1}\right) &= R \ln (r_c), \\ K_1 (T_3 - T_{4s}) + b_v \ln\left(\frac{T_3}{T_{4s}}\right) &= R \ln\left(\frac{r_c}{r}\right), \end{aligned} \tag{8}$$

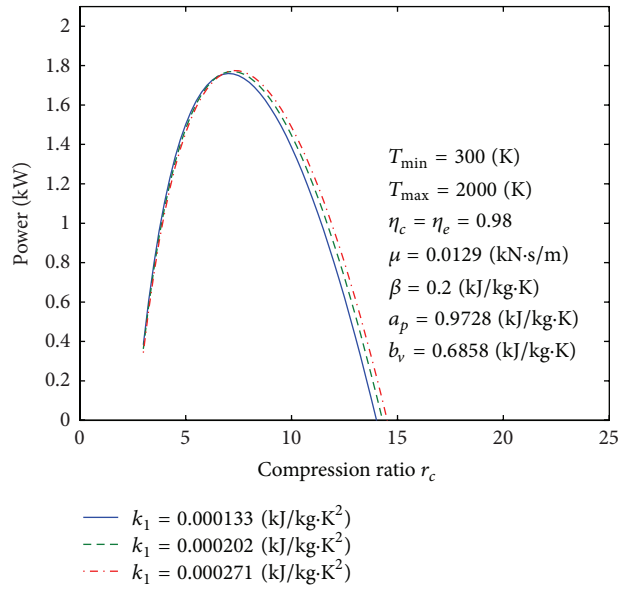

FIGURE 16: Influence of k_1 on curves of the power output versus the compression ratio.

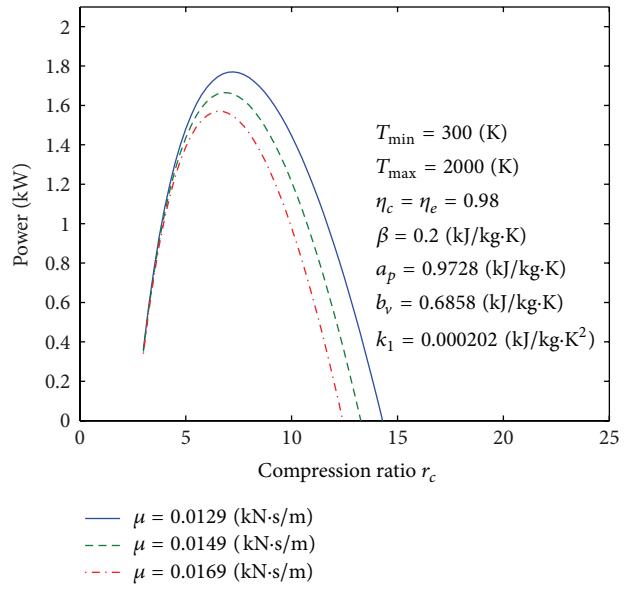

FIGURE 17: Influence of μ on curves of the power output versus the compression ratio.

where the compression ratio, r_c, and the cutoff ratio, r, are defined as

$$r_c = \frac{V_1}{V_2}, \qquad r = \frac{V_3}{V_2}. \tag{9}$$

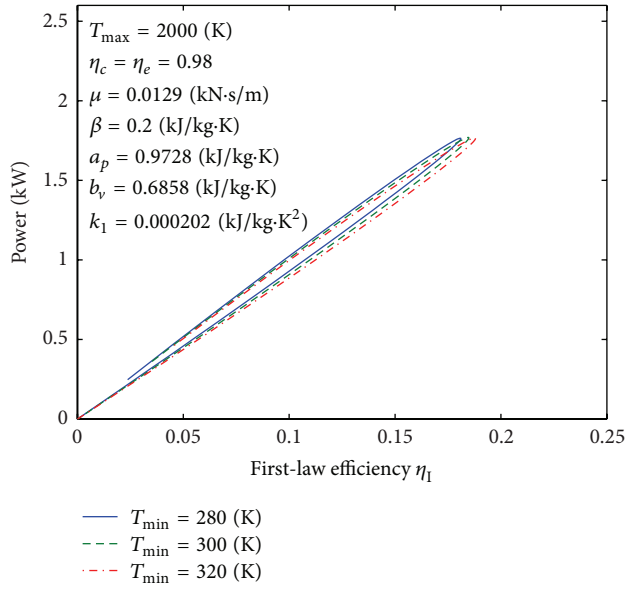

FIGURE 18: Influence of T_{min} on curves of the power output versus the first-law efficiency.

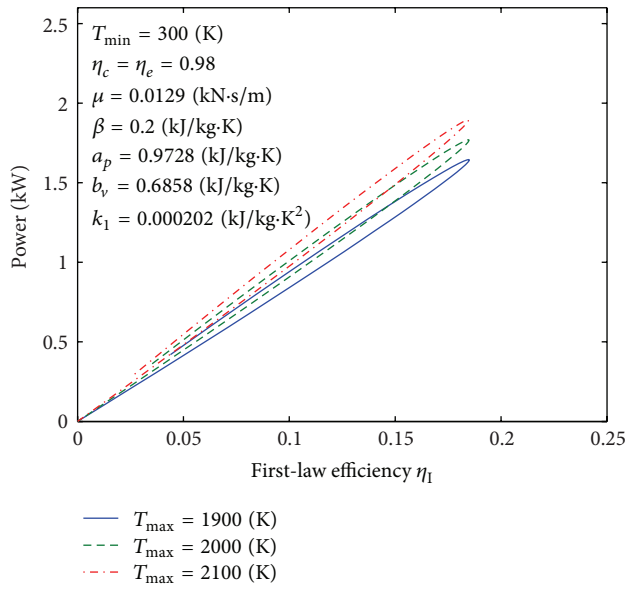

FIGURE 19: Influence of T_{max} on curves of the power output versus the first-law efficiency.

On the other hand, according to (3) and (4), for T_2 and T_4, we have

$$T_2 = \frac{T_{2s} - T_1\left(1 - \eta_c\right)}{\eta_c}, \qquad T_4 = T_{4s}\eta_e + T_3\left(1 - \eta_e\right). \tag{10}$$

The temperatures within the combustion chamber of an internal combustion engine can reach about 2700 (K) and above. Materials in the engine cannot tolerate this kind of high temperature and would quickly fail if proper heat transfer

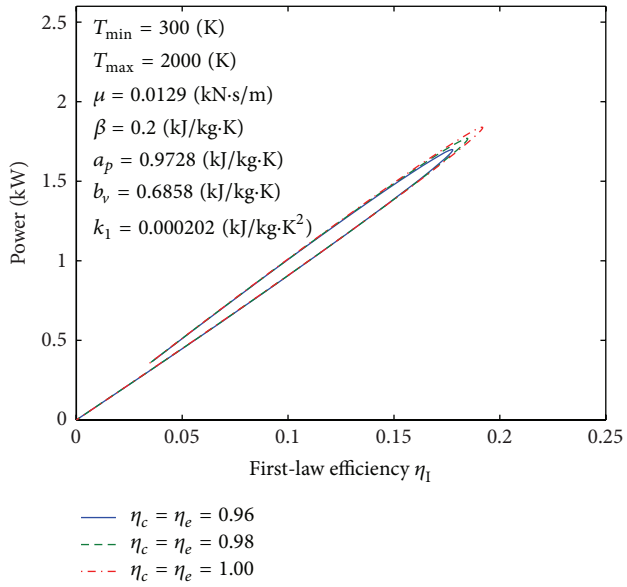

FIGURE 20: Influence of η_c and η_e on curves of the power output versus the first-law efficiency.

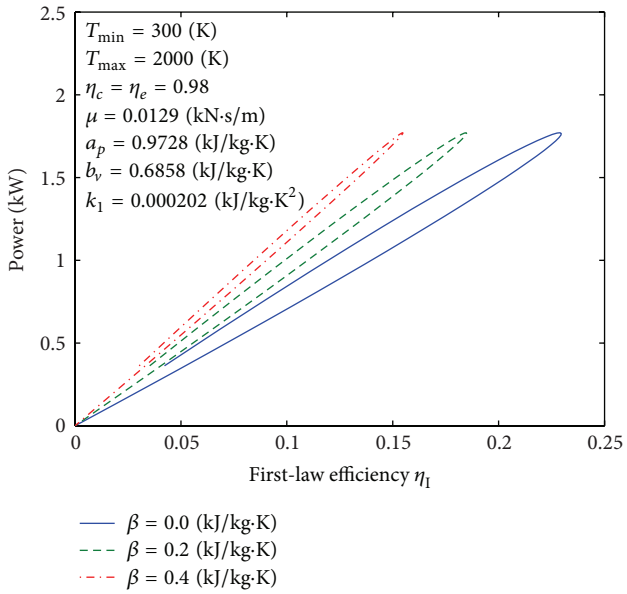

FIGURE 21: Influence of β on curves of the power output versus the first-law efficiency.

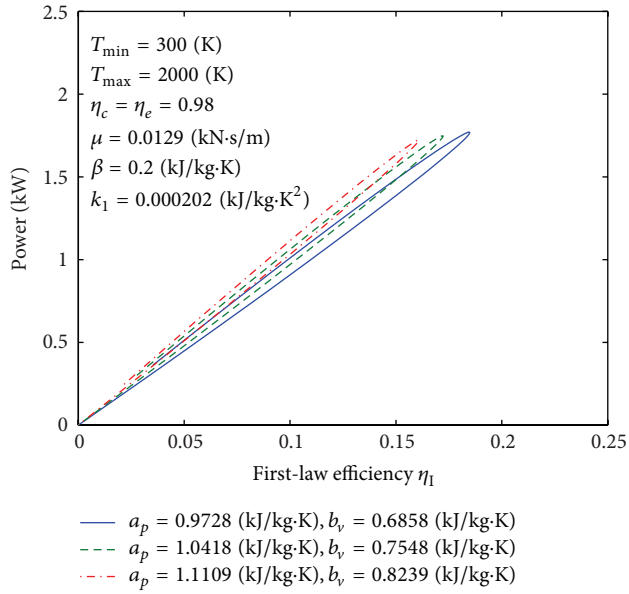

FIGURE 22: Influence of a_p and b_v on curves of the power output versus the first-law efficiency.

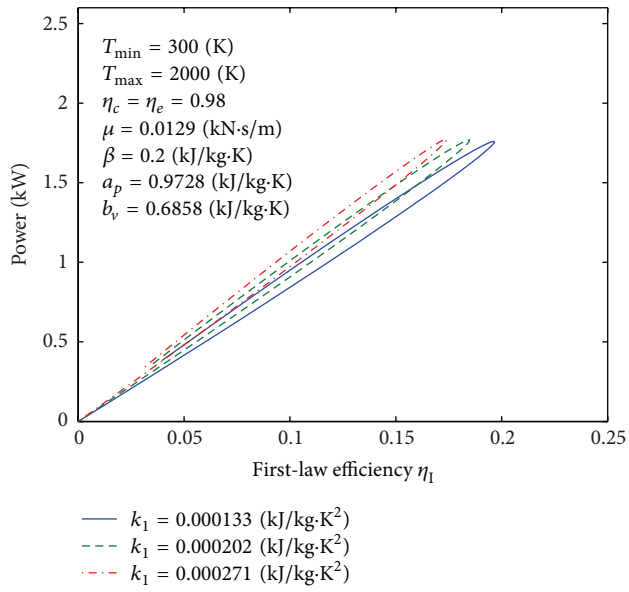

FIGURE 23: Influence of k_1 on curves of the power output versus the first-law efficiency.

does not occur. Therefore to protect the engine from thermal failure, the interior maximum temperature of the combustion chamber must be limited to much lower values by heat fluxes through the cylinder wall during the combustion period. Since during the other processes of the operating cycle, the heat flux is essentially quite small and negligible due to the very short time involved for the processes, it is assumed that the heat loss through the cylinder wall occurs only during combustion. The calculation of actual heat transfer through the cylinder wall occurring during combustion is complex. It is customary therefore to approximate cylinder wall heat transfer flux as being proportional to the average temperature of both the working fluid and cylinder wall, T_0. Furthermore automobile engineers generally assume that, during the operation, the wall temperature remains approximately invariant. The heat released by combustion per second can be obtained as [16]

$$Q_{total} = Q_{in} + Q_{leak}, \tag{11}$$

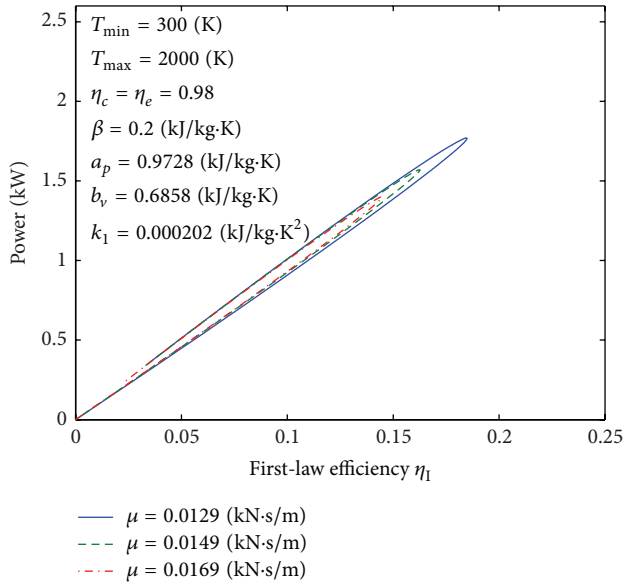

FIGURE 24: Influence of μ on curves of the second-law efficiency versus the first-law efficiency.

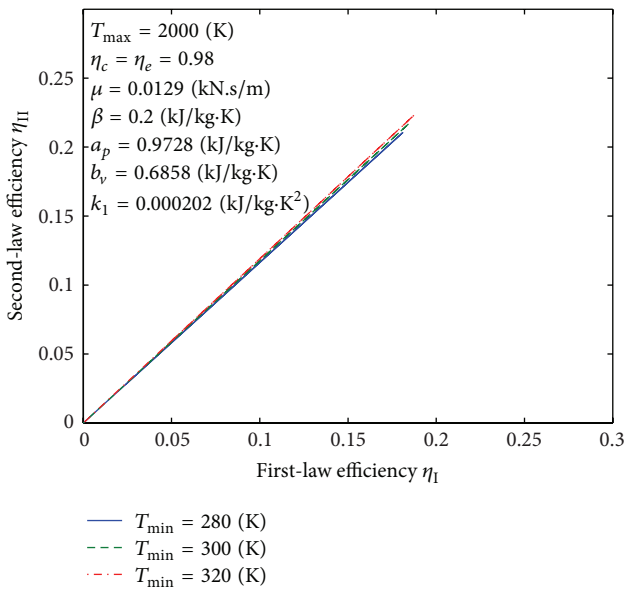

FIGURE 25: Influence of T_{min} on curves of the second-law efficiency versus the first-law efficiency.

where Q_{in} is obtained from (5) and Q_{leak} can be defined as [17]

$$Q_{leak} = MN\left[\beta_1\left(\frac{T_2+T_3}{2}-T_0\right)\right] = MN\left[\beta\left(T_2+T_3-2T_0\right)\right], \quad (12)$$

where, T_0 is the average temperature of the cylinder wall, β_1 is the thermal conductivity between the working fluid and the cylinder wall, and β is the constant related to heat transfer, where $\beta = \beta_1/2$·

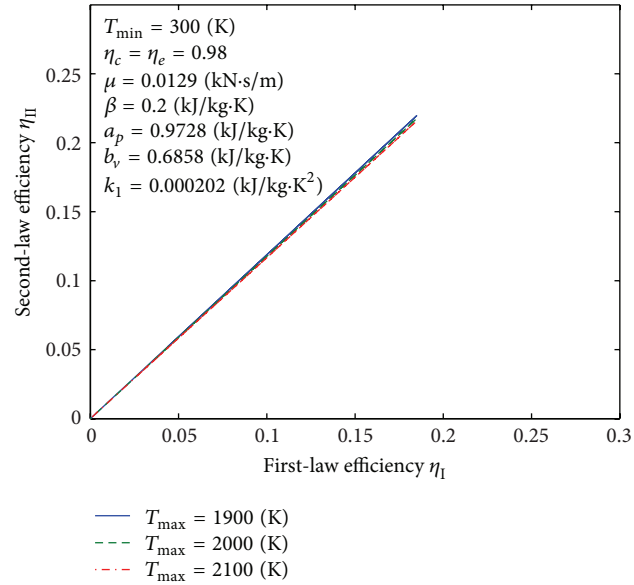

FIGURE 26: Influence of T_{max} on curves of the second-law efficiency versus the first-law efficiency.

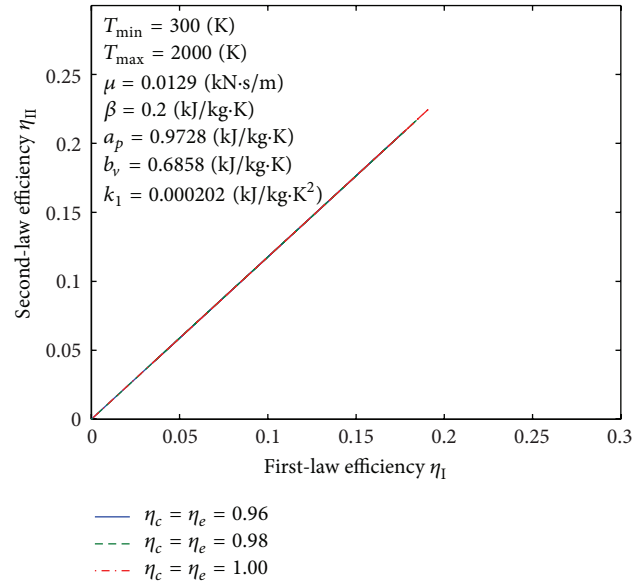

FIGURE 27: Influence of η_c and η_e on curves of the second-law efficiency versus the first-law efficiency.

For the Diesel cycle and assuming a dissipation term represented by a friction force which is a linear function of the velocity gives [17]

$$f_\mu = \mu v = \mu\frac{dx}{dt}, \quad (13)$$

where μ is a coefficient of friction, which takes into account the global losses and x is the piston position. Then, the lost power is

$$P_\mu = \frac{dW_\mu}{dt} = f_\mu\frac{dx}{dt} = \mu\frac{dx}{dt}\frac{dx}{dt} = \mu v^2. \quad (14)$$

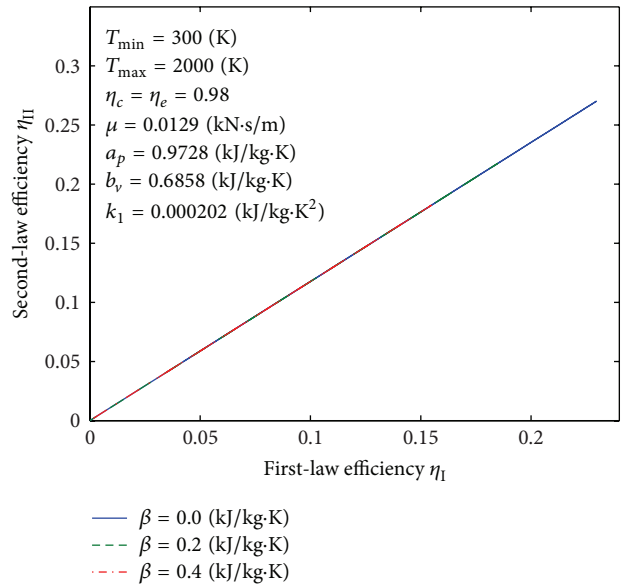

FIGURE 28: Influence of β on curves of the second-law efficiency versus the first-law efficiency.

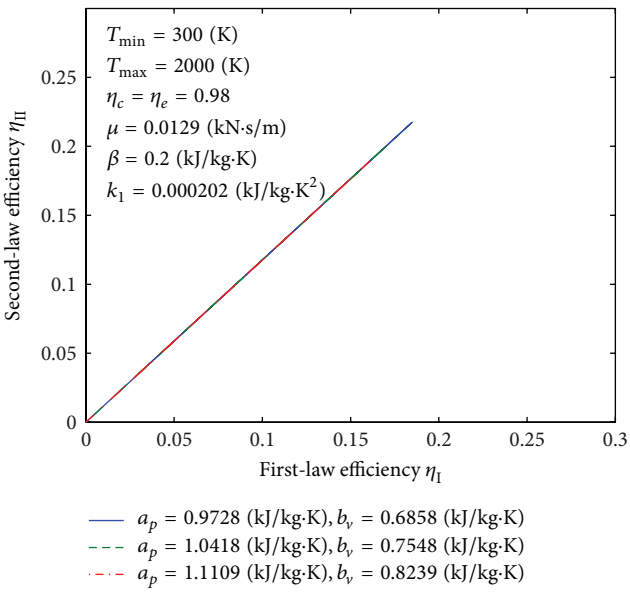

FIGURE 29: Influence of a_p and b_v on curves of the second-law efficiency versus the first-law efficiency.

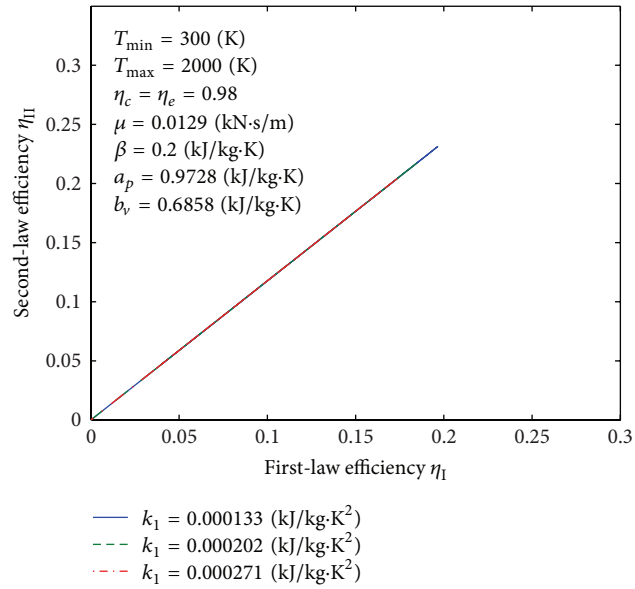

FIGURE 30: Influence of k_1 on curves of the second-law efficiency versus the first-law efficiency.

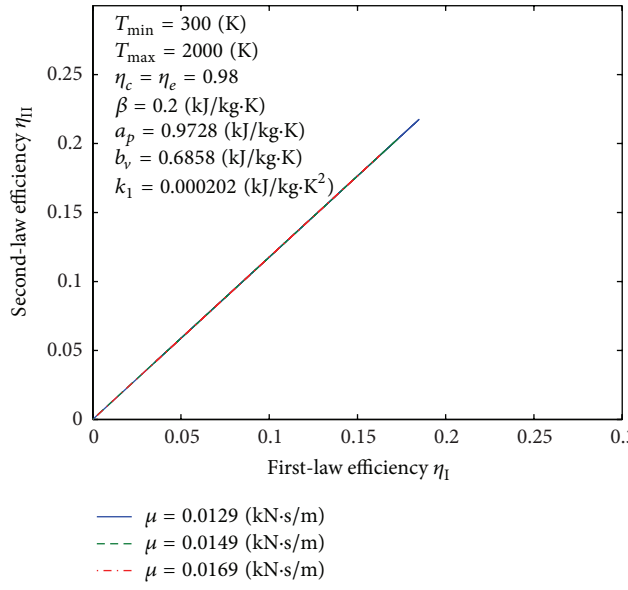

FIGURE 31: Influence of μ on curves of the second-law efficiency versus the first-law efficiency.

If one specifies the engine to be a four-stroke cycle engine, then the total distance the piston travels per cycle is

$$4L = 4\left(x_1 - x_2\right) = 4x_2\left(r_c - 1\right), \tag{15}$$

where x_1 and x_2 are the piston positions at maximum and minimum volumes, respectively.

For a four-stroke cycle engine, running at N cycles per second, the mean velocity of the piston is

$$\overline{v} = 4LN. \tag{16}$$

According to above description, the power output is

$$P = Q_{in} - Q_{out} - P_{\mu}. \tag{17}$$

Finally, the first-law efficiency (thermal efficiency) is

$$\eta_I = \frac{P}{Q_{total}}. \tag{18}$$

2.2. Second-Law Efficiency Analysis. The second-law analysis is a good benchmark for the availability of systems that is described as the ratio of the actual thermal efficiency

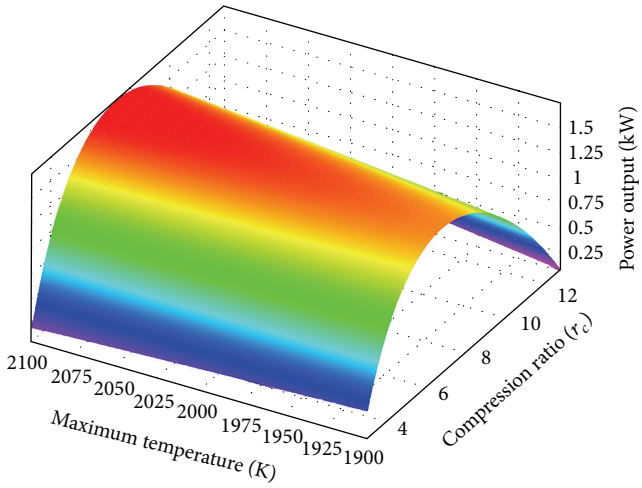

FIGURE 32: 3D continuous layer of power output against maximum temperature and compression ratio when T_{min} = 300 (K), M = 0.000152 (kg), N = 30, k_1 = 0.000202 (kJ/kg·K^2), a_p = 1.0418 (kJ/kg·K), b_v = 0.7548 (kJ/kg·K), $\eta_c = \eta_e$ = 0.98, β = 0.2 (kJ/kg·K), μ = 0.0149 (kN·s/m), and x_2 = 0.01 (m).

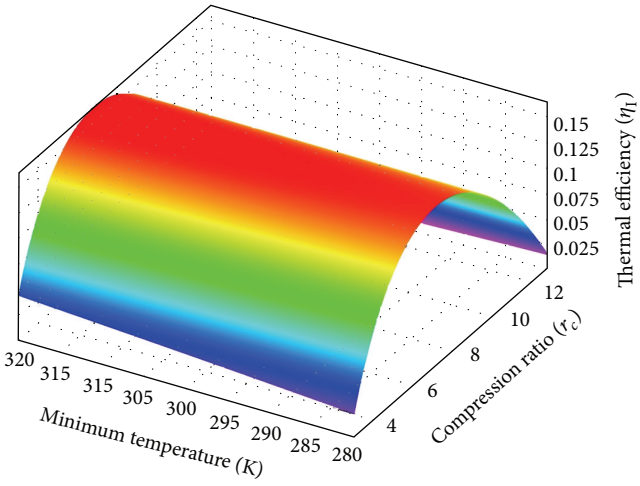

FIGURE 33: 3D continuous layer of thermal efficiency against minimum temperature and compression ratio when T_{max} = 1900 (K), M = 0.000152 (kg), N = 30, k_1 = 0.000202 (kJ/kg·K^2), a_p = 1.0418 (kJ/kg·K), b_v = 0.7548 (kJ/kg·K), $\eta_c = \eta_e$ = 0.98, β = 0.2 (kJ/kg·K), μ = 0.0149 (kN·s/m), and x_2 = 0.01 (m).

(first-law efficiency) to the maximum possible (reversible) thermal efficiency under the same conditions. For the work-producing devices, the second-law efficiency can also be expressed as the ratio of the useful power output to the maximum possible (reversible) power output [1, 3]. According to the above description, the second-law efficiency of an air-standard Diesel cycle is defined as

$$\eta_{II} = \frac{P}{P_{max}} = \frac{\eta_I}{\eta_{max}}, \tag{19}$$

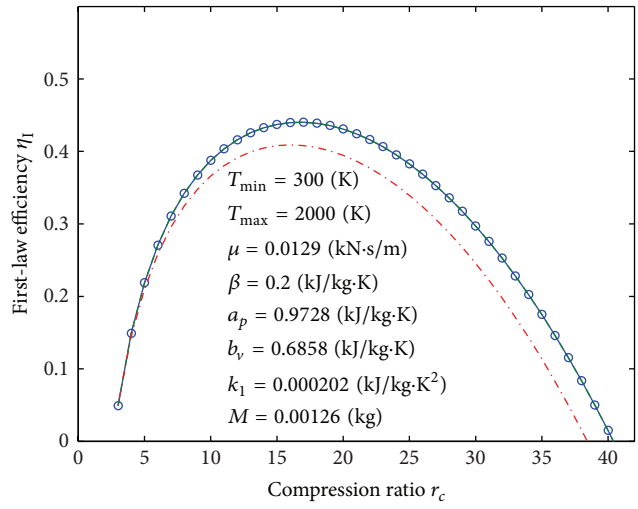

FIGURE 34: A verification compared to [18] (the first-law efficiency versus the compression ratio).

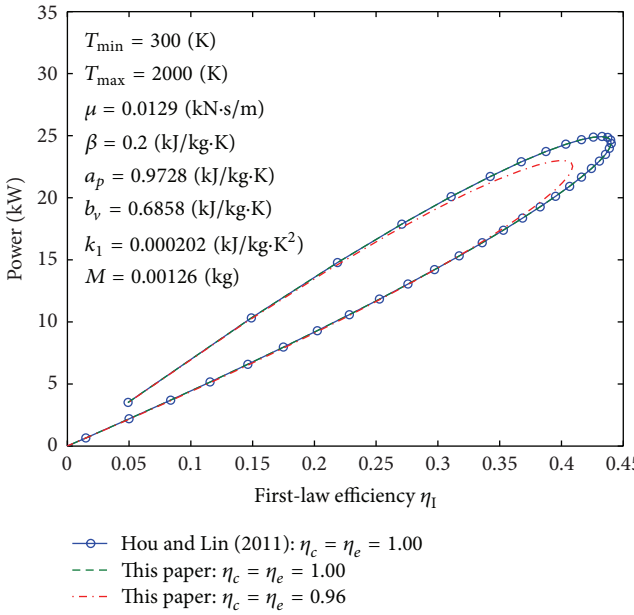

FIGURE 35: A verification compared to [18] (the power output versus the first-law efficiency).

where η_{max} and P_{max} are the maximum possible efficiency (the Carnot efficiency) and the maximum possible power output of the Diesel cycle, respectively, that are defined as follows:

$$\eta_{max} = \left(1 - \frac{T_1}{T_3}\right),$$
$$P_{max} = Q_{total}\eta_{max}. \tag{20}$$

3. Prediction of Thermal Efficiency and Power Output Using Artificial Neural Network

3.1. Artificial Neural Network Theory. The artificial neural networks (ANNs) are a different paradigm for computing. ANNs are based on a parallel architecture to animal brains. They are a form of a multiprocessor computer system by simple scalar messages, simple processing elements, and a high degree of interconnection and adoptive interaction between elements. Multilayer feed forward (MLFF) is the most popular type of ANNs. A diagram of a MLFF neural network is demonstrated in Figure 2. The network includes usually an input layer, some hidden layers, and an output layer. Meanwhile the knowledge is usually stored in connection weights. The process of modifying the connection weights using a suitable learning method is called training:

$$f(x) = \frac{2}{[1 + \exp(-2x)] - 1}. \tag{21}$$

The most widely used learning algorithm of MLFF neural networks is the BEP, a method proposed by McClelland et al. (1987) [27] in a ground-breaking study focused on cognitive computer science.

In this paper, the structure of the ANNs consists of three layers, that is, the input, hidden, and output layers. The magnitudes of ω_{ab} are the weights between the input and the hidden layers and those of ω_{bc} are the weights between the hidden and the output layer. The operation of the BEP method consists of three stages:

(a) feed-forward stage:

$$\begin{aligned} \tau &= \omega_{bc}(n) \cdot y(n), \\ o(n) &= \phi[\tau(n)] = \frac{2}{1 + \exp[-\tau(2n)]}, \end{aligned} \tag{22}$$

where o is the output, τ the input, y the output of hidden layer, and ϕ the activation function,

(b) back-propagation stage:

$$\begin{aligned} \delta(n) &= e(n) \cdot \phi[\tau(n)] \\ &= [d(n) - o(n)] \cdot [o(n)] \cdot [1 - o(n)], \end{aligned} \tag{23}$$

where δ is the local gradient function, e shows the error function, and o and d are the actual and desired outputs, respectively,

(c) adjustable weighted value stage:

$$\begin{aligned} \omega_{ab}(n+1) &= \omega_{ab}(n) + \triangle\omega_{ab}(n) \\ &= \omega_{ab}(n) + \zeta\delta(n) \cdot o(n), \end{aligned} \tag{24}$$

where ζ is the learning rate. Repeating these 3 stages led to a value of the error function, which will be zero or a constant value.

Table 1: Thermodynamic parameters used in this paper.

$a_p = 0.9728 \rightarrow 1.1109$ (kJ/kg·K)	$T_{\min} = 280 \rightarrow 320$ (K)
$b_v = 0.6858 \rightarrow 0.8239$ (kJ/kg·K)	$T_{\max} = 1900 \rightarrow 2100$ (K)
$k_1 = 0.000133 \rightarrow 0.000271$ (kJ/kg·K^2)	$\beta = 0 \rightarrow 0.4$ (kJ/kg·K)
$M = 0.000152$ (kg)	$\mu = 0.0129 \rightarrow 0.0169$ (kN·s/m)
$N = 30$	$\eta_c = 0.96 \rightarrow 1$
$x_2 = 0.01$ (m)	$\eta_e = 0.96 \rightarrow 1$

3.2. Prediction Using Artificial Neural Network. The thermal efficiency and power output prediction parts of this study consist of three steps. First of all a MLFF neural network is created with input, hidden, and output layers, with 2, 10, and 1 neurons, respectively, for each of procedures. The transfer functions for the neurons of hidden and output layers are tansig, defined in (21). The inputs of the ANNs are $T_{\min}$, $T_{\max}$, and r_c, and the target outputs are thermal efficiency and power output. In the next step, the train of ANN is done based on the data of 1600 different conditions using the BEP method. In the training procedure of ANN, the BEP iterations are assumed to be 500. In the BEP training procedure 70%, 20%, and 10% of data are used for training, testing, and verification of neural network, respectively. The training procedures using BEP are shown in Figure 3. As it can be seen, the training procedures have been done with good approximations. In the third step, the trained ANNs are used to predict the thermal efficiency and power output values of conditions which had not been used in the training procedure. The obtained results are also compared with the finite-time thermodynamics results.

4. Results and Discussion

Following [4], the parameters selected for numerical analysis are shown in Table 1. Substituting the parameters and constants of Table 1 into the obtained equations, we can get ranges of temperature of different states, the heat added, the power output, the maximum passible power output, the first-law efficiency, the maximum passible thermal efficiency, and the second-law efficiency in the specified range.

Figures 4, 5, 6, 7, 8, 9, 10, 11, 12, 13, 14, 15, 16, 17, 18, 19, 20, 21, 22, 23, 24, 25, 26, 27, 28, 29, 30, and 31 present selected computations for the effects of the key thermodynamic parameters. When T_1 and T_3 are given, T_{2s} and T_{4s} can be readily obtained via (8); T_2 and T_4 are obtained from (10). Figures 4–10 illustrate the effects of parameters $T_{\min}$, $T_{\max}$, η_c, η_e, β, a_p, b_v, k_1, and μ on the first-law efficiency of the cycle for different values of the compression ratio. It can be seen that the first-law efficiency increases with increasing compression ratio, reaches a maximum value, and then decreases, for fixed value of each one of these parameters. These figures also show that, for $r_c < 10$, the first-law efficiency increases as $T_{\min}$ increases and $T_{\max}$ decreases. For $r_c > 10$, the efficiency increases as $T_{\min}$ decreases and as $T_{\max}$ increases. The compression and expansion efficiencies are between 0.96

Table 2: Comparison of the thermal efficiency results via finite-time thermodynamics and ANN in prediction part when T_{min} = 293 (K), T_{max} = 1900 (K), M = 0.000152 (kg), N = 30, k_1 = 0.000202 (kJ/kg·K^2), a_p = 1.0418 (kJ/kg·K), b_v = 0.7548 (kJ/kg·K), $\eta_c = \eta_e$ = 0.98, β = 0.2 (kJ/kg·K), μ = 0.0149 (kN·s/m), and x_2 = 0.01 (m).

Compression ratio	Finite-time thermodynamics results of thermal efficiency	ANN result of thermal efficiency	Error (%)
3	0.03107245	0.03288305	0.18105927
3.5	0.068272	0.06721445	0.10575547
4	0.09666234	0.09726825	0.06059035
4.5	0.11828659	0.1182551	0.00314946
5	0.13447959	0.13370685	0.07727337
5.5	0.14615507	0.14606122	0.00938465
6	0.15396187	0.15469471	0.07328417
6.5	0.15837449	0.15895983	0.05853451
7	0.15974839	0.15991628	0.0167887
7.5	0.15835523	0.15837659	0.0021353
8	0.1544061	0.15428192	0.01241846
8.5	0.14806734	0.14780046	0.02668725
9	0.13947155	0.13935613	0.01154127
9.5	0.12872552	0.12890096	0.01754379
10	0.11591595	0.11611083	0.01948785
10.5	0.10111369	0.10095862	0.01550761
11	0.08437699	0.08394519	0.04318035
11.5	0.0657539	0.06569867	0.00552299
12	0.04528418	0.04578016	0.04959827

and 1. When these efficiencies are close to 1, the first-law efficiency will increase and vice versa. The first-law efficiency increases as β decreases which is related to heat loss. For $r_c < 13$, the first-law efficiency increases as the invariable parts of the specific heat a_p and b_v decrease; however, for $r_c > 13$, it increases as both of them increase. It is noticed that for $r_c < 12$ or $r_c > 12$ the effect of decreasing or increasing k_1, respectively, will increase the first-law efficiency. As it is expected, reducing the friction parameter μ will enhance the first-law efficiency.

Figures 11–17 show effects of parameters T_{min}, T_{max}, η_c, η_e, β, a_p, b_v, k_1, and μ on the power output of the cycle for different values of the compression ratio. It can be seen that the output power increases with increasing compression ratio, reaches a maximum value, and then decreases, for fixed value of each one of these parameters. For $r_c < 7$, the power output increases as T_{min} increases and T_{max} decreases; and for $r_c > 7$, the power output increases as T_{min} decreases and T_{max} increases. When the compression and expansion efficiencies increase, the power output decreases and vice versa. Based on (12) and (17), parameter β has no direct effect on the power output. For $r_c < 9$, the power output increases as a_p and b_v, that are invariable parts of specific heat, decrease; and for $r_c > 9$, the power output increases as increase of them. For $r_c < 7$ or $r_c > 7$ the effect of decreasing or increasing k_1, respectively, will increase the power output. Similarly, reducing the friction parameter μ will enhance the power output.

Figures 18–24 indicate the influence of parameters T_{min}, T_{max}, η_c, η_e, β, a_p, b_v, k_1, and μ on the power output versus the first-law efficiency, which have a loop shape. The maximum value of the power output corresponds to the maximum value of the first-law efficiency. The first-law efficiency and the power output increase as μ, η_c, and η_e decrease. For fixed value of the power output, the first-law efficiency increases as T_{min} increases and T_{max}, β, a_p, b_v, and k_1 decrease.

Figures 25–31 illustrate effects of the parameters T_{min}, T_{max}, η_c, η_e, β, a_p, b_v, k_1, and μ on the second-law efficiency versus the first-law efficiency. Recall Figures 4–10; the first-law efficiency has the same value at two different compression ratios before it reaches its maximum. With this description in mind, Figures 25–31 indicate that the larger second-law efficiency occurs at the smaller compression ratio. In addition, it can be seen that the first-law and the second-law efficiencies increase as η_c and η_e increase and β, a_p, b_v, k_1, and μ decrease. For fixed value of the first-law efficiency, the second-law efficiency increases as T_{min} increases and T_{max} decreases.

In the prediction part of this study, Tables 2 and 3 show a comparison of the obtained thermal efficiency (first-law efficiency) and power output via ANN and finite-time thermodynamics for different values of compression ratio. As can be seen in these tables, there is an excellent correlation between finite-time thermodynamics and ANN predicted data. So it can be concluded that the proposed procedure based on ANN can be used to interpolate the thermal efficiency and power output values for different conditions. The minimum, maximum, and average value of errors which are defined based on the difference between ANN and finite-time thermodynamics results are 0.0021353%, 0.18105927%,

Table 3: Comparison of the power output results via finite-time thermodynamics and ANN in prediction part when $T_{min} = 293$ (K), $T_{max} = 1900$ (K), $M = 0.000152$ (kg), $N = 30$, $k_1 = 0.000202$ (kJ/kg·K^2), $a_p = 1.0418$ (kJ/kg·K), $b_v = 0.7548$ (kJ/kg·K), $\eta_c = \eta_e = 0.98$, $\beta = 0.2$ (kJ/kg·K), $\mu = 0.0149$ (kN·s/m), and $x_2 = 0.01$ (m).

Compression ratio	Finite-time thermodynamics results of power output	ANN result of power output	Error (%)
3	0.315192303	0.315605633	0.04133292
3.5	0.685703224	0.687118167	0.14149433
4	0.96205101	0.961130499	0.09205105
4.5	1.167368453	1.167782922	0.0414469
5	1.316725308	1.317770379	0.10450705
5.5	1.420420053	1.418476026	0.19440271
6	1.485762847	1.48579036	0.00275124
6.5	1.518105368	1.517966338	0.013903
7	1.521467184	1.520472965	0.09942184
7.5	1.498933296	1.499386913	0.04536175
8	1.452915601	1.451274863	0.16407383
8.5	1.385330151	1.384689729	0.06404215
9	1.297720512	1.298811162	0.10906502
9.5	1.191345593	1.191846543	0.05009502
10	1.067243437	1.066606333	0.06371036
10.5	0.926278388	0.926204827	0.00735607
11	0.769176519	0.770231848	0.10553293
11.5	0.596552631	0.596454221	0.00984107
12	0.408931085	0.408214114	0.07169707

and 0.041549636%, respectively, for thermal efficiency and 0.00275124%, 0.194402708%, and 0.074846647%, respectively, for power output.

In another investigation, the ANNs, that were trained before, are used to plot the 3D continuous layers of thermal efficiency and power output against the maximum and minimum temperatures and compression ratio. Figures 32 and 33 present these layers. The trained ANN can be applied to predict data in points that finite-time thermodynamics data are not available there. Therefore, some data in addition to finite-time thermodynamics data are obtained and then are used to plotting layers. So the layers have been plotted more accurately. Figures 34 and 35 show comparisons [18] of the first-law efficiency versus compression ratio and the output power versus the first-law efficiency, respectively. This comparison shows a good agreement between the current results and those of [18] for the same internal values and constants. Therefore it gives confidence about our results.

5. Conclusions

In this paper, the performance of an air-standard Diesel cycle with consideration of internal irreversibility, variable specific heats of the working fluid, losses due to heat transfer, and friction has been analyzed and the effects of different factors on the first-law efficiency, the power output, and the second-law efficiency have been reported. The obtained results show that the effects of irreversibilities on the performance of the Diesel cycle are obvious and should be considered in practical Diesel cycle analysis. Based on this analysis, the irreversibilities cause strong effects on the performance of the cycle. Meanwhile in this study a procedure has been proposed for prediction of thermal efficiency and power output values using ANN. The comparison of finite-time thermodynamics and ANN results displays that the proposed procedure can be applied to predict the thermal efficiency and power output values for different conditions where the finite-time thermodynamics analysis has not been performed with good correlations.

Nomenclature

a_p: Constant related to specific heat (kJ/kg · K)
b_v: Constant related to specific heat (kJ/kg · K)
C_p: Specific heat at constant pressure (kJ/kg · K)
C_v: Specific heat at constant volume (kJ/kg · K)
d: Desired output of ANN
e: Error function of ANN
f_μ: Friction force (kN)
k: Specific heat ratio
k_1: Constant related to specific heats (kJ/kg · K^2)
L: Stroke (m)
M: Mass of the working fluid (kg)
N: Cycles per second
o: Actual output of ANN
P: Power output of the cycle (kW)
P_μ: Lost power due to friction (kW)
Q_{in}: Heat added to the working fluid per second (kW)

Q_{leak}: Heat leakage through the cylinder wall (kW)
Q_{out}: Heat rejected by the working fluid per second (kW)
Q_{total}: Heat released by combustion per second (kW)
R: Working fluid constant (kJ/kg · K)
r: Cutoff ratio
r_c: Compression ratio
s: Specific entropy (kJ/kg · K)
T_i: Temperature at state i (K)
t: Time (s)
V_i: Volume at state i (m^3)
W_μ: Friction work (kJ)
x_1: Piston position at maximum volume (m)
x_2: Piston position at minimum volume (m)
y: Output of hidden layer of ANN.

Greek Letter

β: Constant related to heat transfer (kJ/kg·K)
β_1: Thermal conductivity between the working fluid and the cylinder wall (kJ/kg·K)
δ: Local gradient function of ANN
η_c: Compression efficiency
η_e: Expansion efficiency
η_I: First-law efficiency
η_{II}: Second-law efficiency
η_{max}: Maximum possible efficiency
μ: Coefficient of friction (kN·s/m)
ν: Velocity of the piston (m/s)
$\bar{\nu}$: Mean velocity of the piston (m/s)
ζ: Learning rate of ANN
τ: Input of ANN
ϕ: Activation function of ANN
ω_{ab}: Weight between the input and the hidden layer of ANN
ω_{bc}: Weight between the hidden and output layer of ANN.

Abbreviations

AI: Artificial intelligence
ANN: Artificial neural network
BEP: Back-error propagation
MLFF: Multilayer feed forward.

Subscript

1, 2, 3, 4: State points.

Conflict of Interests

The authors declare that they have no conflicts of interests.

Acknowledgment

The authors extend their appreciation to the Deanship of Scientific Research at King Saud University for funding this work through the research group Project no. RGP-VPP-080.

References

[1] C. Borgnakke and R. E. Sonntag, *Fundamental of Thermodynamics*, University of Michigan, John Wiley & Sons, 7th edition, 2009.

[2] Y. A. Cengel and M. A. Boles, *Thermodynamics: An Engineering Approach*, McGraw-Hill, New York, NY, USA, 7th edition, 2010.

[3] A. Bejan, *Advanced Engineering Thermodynamics*, John Wiley & Sons, Hoboken, NJ, USA, 2006.

[4] A. Al-Sarkhi, J. O. Jaber, M. Abu-Qudais, and S. D. Probert, "Effects of friction and temperature-dependent specific-heat of the working fluid on the performance of a Diesel-engine," *Applied Energy*, vol. 83, no. 2, pp. 153–165, 2006.

[5] I. Al-Hinti, B. Akash, E. Abu-Nada, and A. Al-Sarkhi, "Performance analysis of air-standard Diesel cycle using an alternative irreversible heat transfer approach," *Energy Conversion and Management*, vol. 49, no. 11, pp. 3301–3304, 2008.

[6] Y. Ge, L. Chen, F. Sun, and C. Wu, "Reciprocating heat-engine cycles," *Applied Energy*, vol. 81, no. 4, pp. 397–408, 2005.

[7] L. Chen, W. Zhang, and F. Sun, "Power, efficiency, entropy-generation rate and ecological optimization for a class of generalized irreversible universal heat-engine cycles," *Applied Energy*, vol. 84, no. 5, pp. 512–525, 2007.

[8] O. A. Ozsoysal, "Heat loss as a percentage of fuel's energy in air standard Otto and Diesel cycles," *Energy Conversion and Management*, vol. 47, no. 7-8, pp. 1051–1062, 2006.

[9] A. Parlak, "Comparative performance analysis of irreversible Dual and Diesel cycles under maximum power conditions," *Energy Conversion and Management*, vol. 46, no. 3, pp. 351–359, 2005.

[10] C. D. Rakopoulos and E. G. Giakoumis, "Second-law analyses applied to internal combustion engines operation," *Progress in Energy and Combustion Science*, vol. 32, no. 1, pp. 2–47, 2006.

[11] N. Lior and N. Zhang, "Energy, exergy, and second law performance criteria," *Energy*, vol. 32, no. 4, pp. 281–296, 2007.

[12] S. K. Som and A. Datta, "Thermodynamic irreversibilities and exergy balance in combustion processes," *Progress in Energy and Combustion Science*, vol. 34, no. 3, pp. 351–376, 2008.

[13] N. Lior and G. J. Rudy, "Second-law analysis of an ideal Otto cycle," *Energy Conversion and Management*, vol. 28, no. 4, pp. 327–334, 1988.

[14] M. M. Rashidi, O. A. Bég, and A. Habibzadeh, "First and second law analysis of an ejector expansion Joule-Thomson cryogenic refrigeration cycle," *International Journal of Energy Research*, vol. 36, no. 2, pp. 231–240, 2012.

[15] M. M. Rashidi, A. Hajipour, and A. Fahimirad, "First and second-laws analysis of an air-standard Dual cycle with heat loss consideration," *International Journal of Mechatronics, Electrical and Computer Technology*, vol. 4, no. 11, pp. 315–332, 2014.

[16] Y. Ge, L. Chen, and F. Sun, "Finite-time thermodynamic modelling and analysis of an irreversible Otto-cycle," *Applied Energy*, vol. 85, no. 7, pp. 618–624, 2008.

[17] Y. Ge, L. Chen, and F. Sun, "Finite-time thermodynamic modeling and analysis for an irreversible Dual cycle," *Mathematical and Computer Modelling*, vol. 50, no. 1-2, pp. 101–108, 2009.

[18] S. S. Hou and J. C. Lin, "Performance analysis of a Diesel cycle under the restriction of maximum cycle temperature with considerations of heat loss, friction, and variable specific heats," *Acta Physica Polonica A*, vol. 120, no. 6, pp. 979–986, 2011.

[19] M. M. Rashidi, A. Mousapour, and A. Hajipour, "Comment on "the effects of heat transfer on the exergy efficiency of an air-standard Otto cycle" by Hakan Özcan, Heat and Mass Transfer (2011) 47:571–577," *Heat and Mass Transfer*, 2014.

[20] S. A. Kalogirou, "Artificial intelligence for the modeling and control of combustion processes: a review," *Progress in Energy and Combustion Science*, vol. 29, no. 6, pp. 515–566, 2003.

[21] M. K. Deh Kiani, B. Ghobadian, T. Tavakoli, A. M. Nikbakht, and G. Najafi, "Application of artificial neural networks for the prediction of performance and exhaust emissions in SI engine using ethanol-gasoline blends," *Energy*, vol. 35, no. 1, pp. 65–69, 2010.

[22] P. Gandhidasan and M. A. Mohandes, "Artificial neural network analysis of liquid desiccant dehumidification system," *Energy*, vol. 36, no. 2, pp. 1180–1186, 2011.

[23] J. Smrekar, M. Assadi, M. Fast, I. Kuštrin, and S. De, "Development of artificial neural network model for a coal-fired boiler using real plant data," *Energy*, vol. 34, no. 2, pp. 144–152, 2009.

[24] M. M. Rashidi, M. Ali, N. Freidoonimehr, and F. Nazari, "Parametric analysis and optimization of entropy generation in unsteady MHD flow over a stretching rotating disk using artificial neural network and particle swarm optimization algorithm," *Energy*, vol. 55, pp. 497–510, 2013.

[25] M. M. Rashidi, N. Galanis, F. Nazari, A. B. Parsa, and L. Shamekhi, "Parametric analysis and optimization of regenerative Clausius and organic Rankine cycles with two feedwater heaters using artificial bees colony and artificial neural network," *Energy*, vol. 36, no. 9, pp. 5728–5740, 2011.

[26] M. M. Rashidi, O. A. Bég, A. B. Parsa, and F. Nazari, "Analysis and optimization of a transcritical power cycle with regenerator using artificial neural networks and genetic algorithms," *Proceedings of the Institution of Mechanical Engineers A: Journal of Power and Energy*, vol. 225, no. 6, pp. 701–717, 2011.

[27] J. L. McClelland, D. E. Rumelhart, and PDP Research Group, *Parallel Distributed Processing*, vol. 2 of *Psychological and Biological Models*, MIT Press, Boston, Mass, USA, 1987.